IEEE Access
Multidisciplinary : Rapid Review : Open Access Journal

Received May 26, 2020, accepted June 6, 2020, date of publication June 22, 2020, date of current version June 30, 2020.

Digital Object Identifier 10.1109/ACCESS.2020.3003285

Predictive Incremental Vector Control for DFIG With Weighted-Dynamic Objective Constraint-Handling Method-PSO Weighting Matrices Design

LUCAS LIMA RODRIGUES[1,2], J. SEBASTIÁN SOLÍS-CHAVES[3], OMAR A. C. VILCANQUI[2], AND ALFEU J. SGUAREZI FILHO[1], (Senior Member, IEEE)

[1]Department of Engineering, Modeling and Applied Social Sciences Center (CECS), Federal University of ABC (UFABC), Santo André 09210-580, Brazil
[2]Center for Exact and Technological Sciences (CCET), Federal University of Acre, Rio Branco 69920-900, Brazil
[3]Department of Mechatronic Engineering, Universidad Escuela Colombiana de Carreras Industriales - ECCI, Bogotá 111311, Colombia

Corresponding author: J. Sebastian Solís-Chaves (jsolisc@ecci.edu.co)

This work was supported in part by the ECCI's University Research Vice Principal Office - Bogotá, Instituto Nacional de Energia Elétrica (INERGE), Coordenação de Aperfeiçoamento de Pessoal de Nivel Superior (CAPES) under Grant 001, in part by the Fundação de Amparo à Pesquisa do Estado de São Paulo (FAPESP) under Grant 2017/04623-3 and Grant 2016/08645-9, and in part by the Conselho Nacional de Desenvolvimento Científico e Tecnológico (CNPq), Brazil, under Grant 405757/2018-2.

ABSTRACT This paper proposes a Particle Swarm Optimization (PSO) based method, the Weighted-Dynamic-Objective Constraint-Handling PSO Method (WDOCHM-PSO). This was used to design the weighting matrices of an incremental Model-Based Predictive Controller (MBPC) for a Doubly Fed Induction Generator (DFIG) applied in a small-scale wind energy system. In contrast to the original PSO, the proposed method has an inner mechanism for dealing with constraints and an adaptive search factor. Additionally, the proposed incremental MPBC implementation does not need the flux information, since the intrinsic integral action rejects the constant flux disturbance. Finally, experimental results show that the proposed controller with the new constraint handling design method is nearly two times faster (In terms of settling time) than other formulations reported in the literature.

INDEX TERMS Doubly-fed induction generator, particle swarm optimization, predictive control, wind energy.

I. INTRODUCTION

During the last decades, there has been a significant effort to reduce the emission of greenhouse gases [1]. As a consequence, wind power penetration has been significantly increased over the last years, and now it represents a major renewable source of energy [2]. Nowadays, Doubly Fed Induction Generators (DFIGs) is one of the most commonly used generators in new turbines [1], and Vector Control (VC) is one of the most popular control approaches for DFIG Rotor Side Converter (RSC) [3]. In summary, this scheme controls active and reactive stator power separately, by decoupling the rotor current d-q synchronous frame [1], [4]. There were proposed several VC schemes for DFIG-based wind turbines, which includes the classical PI [5], Deadbeat Control [6], [7], Neuro-Fuzzy Control [8], [9], Sliding Mode Control (SMC) [10] and Predictive Controllers [11], [12] with good performance.

The associate editor coordinating the review of this manuscript and approving it for publication was Zhouyang Ren.

The predictive control theory describes a set of controllers that uses the future behavior of the system to decide the best action to reach an objective by using the minimization of a cost function. The estimation of future behavior is determined by a mathematical model combined with actual and past measurements of the system. Predictive control for power converters and motor drives is divided into two categories: finite or continuous control set. Finite control set directly uses as a control input one of the eight possible space vector signals, considering a two level voltage source converter, under optimization process [3], [13], [14], and the continuous control set that uses a modulated control signal [15]. To reach this objective, the DFIG system can be modeled as a space state equation [16], [17], by using a transfer function of the system [11], [18], [19], non-linear mathematical models [20] or continuous time models [21].

The non-linear models are useful in many applications [22]–[24], because it implies a better representation of the real system. However, it increases the computational cost, which is critical in real-time systems with a low-cost DSP, especially when it uses high-frequency rates, which is DFIG's case. Therefore, there are some works with non-linear models but limited to simulations [20], [25], [26]. An interesting alternative is the adaptive robust control [27], due to its capability to deal with structured and unstructured uncertainties, especially to deal with fault operation conditions produced by voltage sags.

Even though MBPC minimizes the cost function, there is not an absolute rule that guarantees that the minimal predicted is in fact, a high-quality solution for a real plant, this is owing to the fact that the models are always an approximation of a physical system. Increasing the model complexity could reduce this approximation gap; however, the complex models have a relatively high on-line computational burden, which is critical for drive applications [28]–[30]. A possible solution to overcome the trade-off between the MBPC accuracy and its associated computational cost is to use a simple prediction model injunction with additional off-line optimization of a high-fidelity model. In the case of the MBPC, off-line optimization is related to the cost function parameters [31].

The Particle Swarm Optimization (PSO) is considered efficient for complex problems optimization because it lies in a simple programming concept and not require an objective function and/or a model to be differentiable or continuous [32]. Regarding DFIG, PSO was used to design of different controllers as classical PI/PID controllers [33], [34], discrete-time inverse optimal controller [35] and Sliding Mode Controller [36], as an alternative for the classical design.

In spite of the unnumerous advantages of PSO to optimize complex problems, in its original form, this algorithm lacks an inner mechanism for dealing with constraints. In [37], it was proposed the Dynamic-Objective Constraint-Handling Method (DOCHM) PSO, which transforms the original constrained objective function into two unconstrained problems. This method is bi-objective and deals with both unconstrained functions. However, this method uses two search region and it can degrade the convergence speed because the optimization needs to be done twice. In order to increase the convergence speed of DOCHM and overcome the problem of premature convergence, we include the adaptive inertia [38] in DOCHM. So in the beginning, the algorithm can find a high-quality solution fast, then in the later iterations the algorithm increases the search capacity, avoiding premature convergences. The new method is renamed as Weighted-Dynamic-Objective Constraint-Handling Method (WDOCHM).

Using the philosophy of low-cost MPBC algorithm injunction with PSO off-line optimization, a novel application of an MBPC with an incremental state-space model and an infinite control set for DFIG, is proposed in this paper. In other words, there is an online optimization that is a characteristic of predictive control, and another offline optimization that uses a more complex optimization problem. This later optimization can be reduced trough the low-cost optimization problem, commonly used in MBPC theory. The prediction model has the advantage to eliminate the flux component under predictions because this component is modeled as a constant disturbance. Here, a novel method is proposed to design weighting matrices using the novel WDOCHM-PSO. Finally, the results obtained in an experimental setup endorse this proposal.

II. DFIG MODEL-BASED PREDICTIVE CONTROL

A. ROTOR SIDE INCREMENTAL MODEL

As explained in [1], [4], [16], DFIG stator flux oriented vector control is a strategy used on RSC to control the stator active and reactive power separately. This strategy uses the information from the stator flux, $\vec{\lambda}_s$, to synchronize the plant space vectors in a stator flux reference frame and it controls rotor current direct and quadrature components. Since $\vec{\lambda}_s^s$ is oriented in its own reference frame, $\lambda_{sd}^s = |\vec{\lambda}_s|$ and $\lambda_{sq}^s = 0$ [4], [16]. Here, the subscripts d and q denote direct and quadrature components.

Assuming that stator voltage imposes the flux, $\vec{v}_s^s \approx -j\omega_s\vec{\lambda}_s^s$, making possible to derive the following state-space matrix DFIG model, as is described in [4], [16]:

$$\underbrace{\begin{bmatrix} \dfrac{di_{rd}^s}{dt} \\ \dfrac{di_{rq}^s}{dt} \end{bmatrix}}_{\frac{dx}{dt}} = \underbrace{\begin{bmatrix} -\dfrac{R_r}{\sigma L_r} & \omega_{sl} \\ -\omega_{sl} & -\dfrac{R_r}{\sigma L_r} \end{bmatrix}}_{A} \underbrace{\begin{bmatrix} i_{rd}^s \\ i_{rq}^s \end{bmatrix}}_{\boldsymbol{x}} + \underbrace{\begin{bmatrix} \dfrac{1}{\sigma L_r} & 0 \\ 0 & \dfrac{1}{\sigma L_r} \end{bmatrix}}_{B} \times \underbrace{\begin{bmatrix} v_{rd}^s \\ v_{rq}^s \end{bmatrix}}_{\boldsymbol{u}} + \underbrace{\begin{bmatrix} 0 \\ -\dfrac{\omega_{sl} L_m}{\sigma L_s L_r}|\vec{\lambda}_s| \end{bmatrix}}_{\boldsymbol{w}} \tag{1}$$

$$\underbrace{\begin{bmatrix} y_d \\ y_q \end{bmatrix}}_{\boldsymbol{y}} = \underbrace{\begin{bmatrix} 1 & 0 \\ 0 & 1 \end{bmatrix}}_{C} \boldsymbol{x} \tag{2}$$

and the relationship between the components of the rotor current vector and the reactive Q_s and active P_s power is done by:

$$i_{rq}^s = -\frac{2L_s}{3L_m|\vec{v}_s^s|}P_s \text{ and } i_{rd}^s = \frac{|\vec{\lambda}_s^s|}{L_m} - \frac{2L_s}{3L_m|\vec{v}_s^s|}Q_s \tag{3}$$

where $\boldsymbol{x}, \boldsymbol{u}, \boldsymbol{y}$ are plant states, inputs and outputs, respectively. Additionally, $\boldsymbol{w}$ represents a disturbance intrinsic to the system, due to the stator flux and the slip speed, s superscript denotes that the variable is oriented in stator flux referential, $\vec{i}_r$, $\vec{v}_r$, $\vec{v}_s$ and $\vec{\lambda}_s$ are rotor current, rotor voltage, stator voltage and stator flux space-vectors, respectively. L_r, L_s, L_m represent rotor, stator and magnetizing inductances, and R_r represents rotor resistance. Also, $\omega_{sl} = \omega_s - p\omega_m$ denotes the slip speed, where p is the number of pair of poles, ω_m is the mechanical shaft speed and ω_s is the grid frequency. And finally, $\sigma = 1 - \frac{L_m^2}{L_s L_r}$ is the total leakage factor.

Because $|\vec{\lambda}_s|$ is approximately constant, $\boldsymbol{w}$ is considered constant. Moreover, Eq. (4) gives the discrete state-space model using a Zero-Order-Hold (ZOH) with no delay and T sample period [4], [16], [39].

$$\begin{aligned} \boldsymbol{x}(k+1) &= A_d(\omega_{sl}(k))\boldsymbol{x}(k) + B_d\boldsymbol{u}(k) + \boldsymbol{w_d}(k) \\ \boldsymbol{y}(k) &= C_d\boldsymbol{x}(k) \end{aligned} \tag{4}$$

where:

$$\begin{aligned} A_d(\omega_{sl}) &= e^{AT} \approxeq I + AT = \begin{bmatrix} 1 - \dfrac{R_rT}{\sigma L_r} & \omega_{sl}(k)T \\ -\omega_{sl}(k)T & 1 - \dfrac{R_rT}{\sigma L_r} \end{bmatrix} \\ B_d &= \int_0^T e^{A\tau}Bd\tau \approxeq BT = \begin{bmatrix} \dfrac{T}{\sigma Lr} & 0 \\ 0 & \dfrac{T}{\sigma Lr} \end{bmatrix} \\ C_d &= C \end{aligned} \tag{5}$$

and $\boldsymbol{w_d}(k)$ is the discretized version of $\boldsymbol{w}$. As the mechanical time constant is much higher than the electrical time constant, ω_{sl} is approximately constant compared to the electrical dynamics. Thus, the DFIG state-space model can be linearized for each sample period in the matrix $A_d(\omega_{sl})$, using the measured slip speed in instant k, that is $\omega_{sl}(k)$ [4], [40].

According to [41], an incremental state-space model is expressed in terms of the state variables changes $\boldsymbol{\Delta x}(k) = \boldsymbol{x}(k) - \boldsymbol{x}(k-1)$ and inputs, $\boldsymbol{\Delta u}(k) = \boldsymbol{u}(k) - \boldsymbol{u}(k-1)$, which is represented by the following augmented state-space model [41], [42]:

$$\begin{aligned} \underbrace{\begin{bmatrix} \boldsymbol{\Delta x}(k+1) \\ \boldsymbol{y}(k+1) \end{bmatrix}}_{\xi(k+1)} &= \underbrace{\begin{bmatrix} A_d(\omega_{sl}) & 0 \\ C_dA_d(\omega_{sl}) & I \end{bmatrix}}_{A_a(\omega_{sl})} \underbrace{\begin{bmatrix} \boldsymbol{\Delta x}(k) \\ \boldsymbol{y}(k) \end{bmatrix}}_{\xi(k)} \\ &\quad + \underbrace{\begin{bmatrix} B_d \\ C_dB_d \end{bmatrix}}_{B_a} \boldsymbol{\Delta u}(k) + \Delta \boldsymbol{w_d}(k) \\ \boldsymbol{y}(k) &= \underbrace{\begin{bmatrix} 0 & I \end{bmatrix}}_{C_a} \underbrace{\begin{bmatrix} \boldsymbol{\Delta x}(k) \\ \boldsymbol{y}(k) \end{bmatrix}}_{\xi(k)} \end{aligned} \tag{6}$$

where $\xi(k+1)$ is the augmented state variables, and A_a,[1] B_a, C_a are augmented matrices related to the incremental state-space model. Since the changes in flux disturbance are null, the terms of $\Delta \boldsymbol{w_d}(k) = \boldsymbol{w_d}(k) - \boldsymbol{w_d}(k-1)$ were suppressed in Eq. (6). This is possible due to the flux perturbation is constant, and $\Delta \boldsymbol{w_d}(k) = \boldsymbol{w_d}(k) - \boldsymbol{w_d}(k-1) \approx 0$. The model simplification by removing the flux influence, is one of the advantages of the incremental state-space model proposed here.

[1]To simplify the notation we are going to use A_a instead of $A_a(\omega_{sl})$.

B. DFIG INCREMENTAL PREDICTIVE CONTROL

Prediction of the future outputs is possible by advancing and iterating Equation (6). This is shown in Equation (7), and is explained with more detail in [31]:

$$\begin{aligned} \boldsymbol{y}(k+1) &= C_aA_a\xi(k) + C_aB_a\boldsymbol{\Delta x}(k) \\ \boldsymbol{y}(k+2) &= C_aA_a^2\xi(k) + C_aA_aB_a\boldsymbol{\Delta x}(k) \\ &\quad + C_aB_a\boldsymbol{\Delta x}(k+1) \\ &\vdots \end{aligned} \tag{7}$$

Finally, repeating and rewriting this process many times, all the predicted outputs are obtained in a compact matrix format, that is:

$$\mathcal{Y} = \mathcal{A}\xi(k) + \mathcal{B}\Delta\mathcal{U} \tag{8}$$

where:

$$\begin{aligned} \mathcal{Y} &= \begin{bmatrix} \boldsymbol{y}(k+1) & \boldsymbol{y}(k+2) & \cdots & \boldsymbol{y}(k+N_y) \end{bmatrix}^T \\ \Delta\mathcal{U} &= \begin{bmatrix} \boldsymbol{\Delta u}(k) & \boldsymbol{\Delta u}(k+1) & \cdots \boldsymbol{\Delta u}(k+N_u-1) \end{bmatrix}^T \\ \mathcal{A} &= \begin{bmatrix} C_aA_a & C_aA_a^2 & \cdots & C_aA_a^{N_y} \end{bmatrix}^T \\ \mathcal{B} &= \begin{bmatrix} C_aB_a & 0 & \cdots & 0 \\ C_aA_aB_a & C_aB_a & \cdots & 0 \\ \vdots & \vdots & \ddots & \cdots \\ C_aA_a^{N_y-1}B_a & C_aA_a^{N_y-2}B_a & \cdots & C_aA_a^{N_y-N_u}B_a \end{bmatrix} \end{aligned} \tag{9}$$

In Eq. (8) and Eq. (9), $\Delta\mathcal{U}$ and $\mathcal{Y}$ represent all predicted input increments and outputs, respectively. $\mathcal{A}$ and $\mathcal{B}$ are matrices that in turn contain matrices A_a, B_a and C_a. Furthermore, N_y is considered as the prediction whereas N_u is the control horizon, respectively.

Initially, the incremental prediction model is linearized considering the current ω_{sl}. Then, this model is used to calculate a quadratic cost function, given by Eq. (10). This is described in [31], [43] and [44]. Afterward, the permanence index is minimized and the corresponding control law can be obtained, as follows:

$$\begin{aligned} J = \sum_{i=1}^{N_y} \boldsymbol{E}(k+i)^T W_y \boldsymbol{E}(k+i) \\ + \sum_{j=0}^{N_u-1} \boldsymbol{\Delta u}(k+j)^T W_u \boldsymbol{\Delta u}(k+j) \end{aligned} \tag{10}$$

Here, $\boldsymbol{E}(k+i) = \boldsymbol{y}(k+i) - \boldsymbol{y}_{\mathrm{ref}}(k+i)$ represents the predicted errors, $W_y = \begin{bmatrix} W_{y,11} & W_{y,12} \\ W_{y,21} & W_{y,22} \end{bmatrix}$ and $W_u = \begin{bmatrix} W_{u,11} & W_{u,12} \\ W_{u,21} & W_{u,22} \end{bmatrix}$ are weighting matrices related to the predicted errors and predicted inputs, $\boldsymbol{y}_{\mathrm{ref}}(k+i)$ are the future references, which are considered constant, during all the prediction period. The input applied by the controller is the minimal solution of Eq. (10) or, in an analytical point of view, when $\nabla_{\boldsymbol{\Delta u}} J = 0$. The result of this minimization is the following control

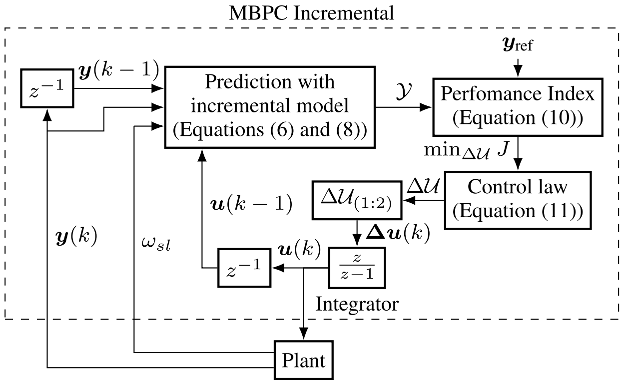

FIGURE 1. **MBPC Incremental diagram.**

law $\Delta\mathcal{U}$, as is depicted in [43]:

$$\Delta\mathcal{U} = (\mathcal{B}^T\mathcal{W}_y\mathcal{B} + \mathcal{W}_u)^{-1}\mathcal{B}^T\mathcal{W}_y\left(\mathcal{Y}_{\text{ref}} - \mathcal{A}\xi(k)\right) \quad (11)$$

where $\mathcal{W}_y$, $\mathcal{W}_u$ are main diagonal repetition of matrices W_y and W_u, and

$$\begin{aligned}\mathcal{Y}_{\text{ref}} &= \begin{bmatrix}\boldsymbol{y}_{\text{ref}}(k+1) & \cdots & \boldsymbol{y}_{\text{ref}}(k+N_y)\end{bmatrix}^T \\ &= \boldsymbol{y}_{\text{ref}}(k+1)\begin{bmatrix}1 & 1 & \cdots & 1\end{bmatrix}^T\end{aligned} \quad (12)$$

are the outputs references, respectively.

The MBPC Incremental block diagram presented in Fig. 1 summarize the proposed incremental method.

In Fig. 1 just the control action related to the next sample time is applied to the plant. It means that only the first two elements of $\Delta\mathcal{U}$, or the $\Delta\mathcal{U}_{(1:2)}$, in junction with $\boldsymbol{\Delta u}(k) = [\,\Delta\mathcal{U}_1\ \Delta\mathcal{U}_2\,]^T$, are currently used. After this, the output increment is integrated before it goes to the plant, giving as result $u(k)$.

Concluding, the block diagram of the complete control strategy is shown in Fig. 2. In this figure, the *abc* superscript represent three-phases variables, $P_{s,\text{ref}}$ and $Q_{s,\text{ref}}$ are the active and reactive power references. In addition, a Space-Vector Pulsed-width Modulator (SVPWM) is applied to modulated voltage in the RSC, as is depicted in [4].

C. MBPC INCREMENTAL CLOSED-LOOP ANALYSIS

This sub-section deals with the controller-plant closed-loop transfer matrix equivalent and thus analyze the controller behavior under lower frequencies, constant errors, and/or disturbances.

Firstly, Eq. (11) is rewritten in terms of the gain $\mathcal{K} = (\mathcal{B}^T\mathcal{W}_y\mathcal{B} + \mathcal{W}_u)^{-1}\mathcal{B}^T\mathcal{W}_y$:

$$\Delta\mathcal{U} = \mathcal{K}\left(\mathcal{Y}_{\text{ref}} - \mathcal{A}\xi(k)\right) \quad (13)$$

Sequentially, the control law is defined as follows:

$$\boldsymbol{\Delta u} = \tilde{\mathcal{K}}\left(\mathcal{Y}_{\text{ref}} - \mathcal{A}\xi(k)\right) \quad (14)$$

where

$$\tilde{\mathcal{K}} = \begin{bmatrix}\mathcal{K}_{(1)} & \ldots & \mathcal{K}_{(n_y)}\end{bmatrix} \quad (15)$$

is the first two lines of $\mathcal{K}$. Also, in Equation (15), $K_{(i)} \in \mathbb{R}^{2\times 2}$ are square matrices.

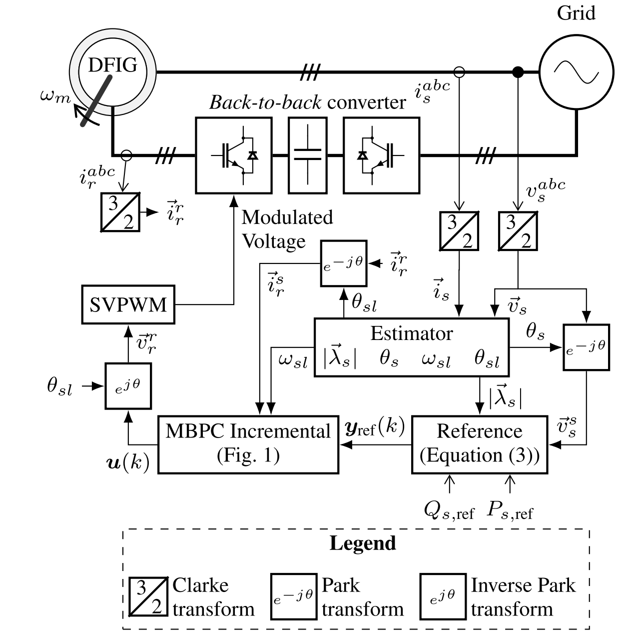

FIGURE 2. **DFIG rotor side converter control diagram.**

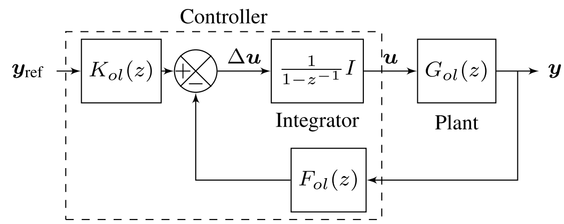

FIGURE 3. **Block diagram of (16) and (18).**

Alternatively:

$$\Delta\boldsymbol{u} = K_{ol}(z)\boldsymbol{y}_{\text{ref}} - F_{ol}(z)\boldsymbol{y} \quad (16)$$

where:

$$\begin{aligned}F_{ol}(z) &= \sum_{i=1}^{n_y}\mathcal{K}_{(i)}\left(I + \sum_{j=0}^{i-1}A_d^{i-j} - z^{-1}\sum_{j=0}^{i-1}A_d^{i-j}\right)\\ K_{ol}(z) &= \sum_{i=1}^{n_y}\mathcal{K}_{(i)}\end{aligned} \quad (17)$$

and the plant transfer matrix is calculated using:

$$G_{ol} = (zI - A_d)\,B_d^{-1} + G_d \quad (18)$$

where:

$$G_d = \begin{bmatrix}0 & 0\\ -\dfrac{\omega_{sl}L_m}{\sigma L_s L_r}T|\vec{\lambda}_s| & 0\end{bmatrix} \quad (19)$$

Also, in Fig. 3 the equivalent diagram of Eq. (16) and Eq. (18) are shown.

The closed loop transfer matrix of Fig. 3 is presented in Eq. (20).

$$G_{cl} = K_{ol}I_{ol}G_{ol}\left(I + F_{ol}I_{ol}G_{ol}\right)^{-1} \quad (20)$$

where $I_{ol}(z) = \frac{1}{1-z^{-1}}I$ is an integrator.

The presence of the integrator in the inner loop of Fig. 3 and in Eq. (20) indicates that the controller has a pole in the unitary circle, which means that the controller has a very high gain for the error $\Delta \boldsymbol{u}$, avoiding steady-state errors caused by low frequency or constant disturbances, as the flux component [45].

III. DESIGN OF WEIGHTING MATRICES USING PSO

PSO is inspired by the social and cooperative behavior presented in several species, as birds and fishes. This algorithm tries to minimize a fitness function, and each particle represents a potential solution to the optimization problem. During each PSO iteration, particles move in the direction of the optimal solution [46].

A. OPTIMIZATION PROBLEM AND FITNESS FUNCTION

The system works inside the linear region. In this situation, the operation point is proportional to the slip speed variation and the stator flux. Furthermore, the controller linearizes at each iteration, by inputting current slip speed. So, to simplify this idea, it can be noticed that the controller uses the constant shaft speed and the step response, as input references.

The Integral Absolute Magnitude of Error (ITAE) of both direct, ITAE_d, and quadrature components, ITAE_q, was used to bench-marking the current responses. The performance index is commonly used as a guideline to tuning the controller parameters [33], [47].This criterion has some interesting advantages, it can be mentioned, among others, that is more selective, produce less overshoot and oscillation than Integral Square Error (ISE) and Integral of Absolute Error (IAE) and in accord with criteria described in [48]–[50], it can be defined as follows:

$$\begin{aligned}\mathrm{ITAE}_d = &\int_{t_{\mathrm{step}_d}=1}^{t_{\mathrm{step}_d}+0.49} (t - t_{\mathrm{step}_d})|E_d(t)|dt \\ &+ \int_{t_{\mathrm{step}_q}=1.5}^{t_{\mathrm{step}_q}+0.49} (t - t_{\mathrm{step}_q})|E_d(t)|dt \end{aligned} \tag{21}$$

$$\begin{aligned}\mathrm{ITAE}_q = &\int_{t_{\mathrm{step}_q}=1.5}^{t_{\mathrm{step}_q}+0.49} (t - t_{\mathrm{step}_q})|E_q(t)|dt \\ &+ \int_{t_{\mathrm{step}_d}=1}^{t_{\mathrm{step}_d}+0.49} (t - t_{\mathrm{step}_d})|E_q(t)|dt \end{aligned} \tag{22}$$

where $t_{\mathrm{step}_d} = 1$ s and $t_{\mathrm{step}_q} = 1.5$ s are the instants of time where the step function is applied, under direct and quadrature components. $E_d(t) = i^s_{rd,\mathrm{ref}}(t) - i^s_{rd}(t)$, $E_q(t) = i^s_{rq,\mathrm{ref}}(t) - i^s_{rq}(t)$ are the errors of the direct and quadrature components.

As constraints of the optimization problem, the direct, $M_{p,d} < 35\%$, the quadrature, $M_{p,q} < 35\%$, the current overshoots, the direct, $t_{ss,d} < 3$ ms, the quadrature, $t_{ss,q} < 3$ ms and the setting time, were used.

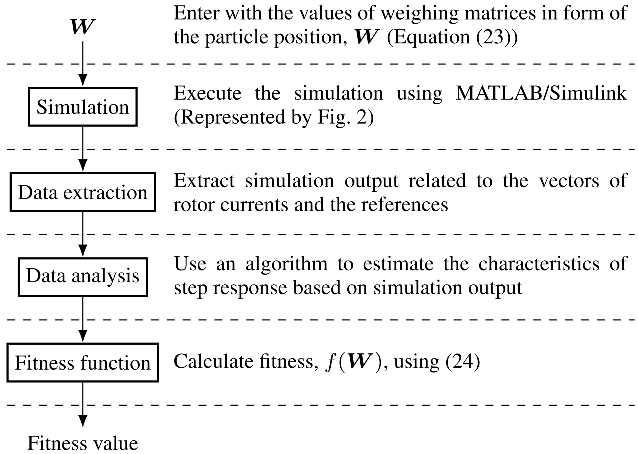

FIGURE 4. Step by step of fitness function.

Each particle position, or the variable to be optimized, $\boldsymbol{W}$, is a vector that includes the elements of MBPC weighting matrices:

$$\begin{aligned}\boldsymbol{W} &= \left[W_{y,11}, W_{y,12}, \ldots, W_{u,21}, W_{u,22}\right]^T \\ &= \left[W_1, W_2, \ldots, W_8\right]^T \end{aligned} \tag{23}$$

Hence, the optimization problem, or the guidelines for the controller tuning, is defined as:

$$\begin{aligned} &\underset{\boldsymbol{W}\in\mathbb{S}}{\text{minimize}} f(\boldsymbol{W}) = \max\left(\left\{\mathrm{ITAE}_d, \mathrm{ITAE}_q\right\}\right) \\ &\text{subject to } \boldsymbol{M}_{p,d} \text{ and } \boldsymbol{M}_{p,q} < 35\% \\ &\qquad\qquad \boldsymbol{t}_{ss,d} \text{ and } \boldsymbol{t}_{ss,q} < 3 \text{ ms} \end{aligned} \tag{24}$$

where $\mathbb{S}$ is the search space, or, in other words, the objective function domain.

In short, the algorithm of fitness function runs the model described in Fig. 2, using a simulation of electrical system, and it analyzes the step response for references of direct, $i^s_{rd,\mathrm{ref}}$, and quadrature, $i^s_{rq,\mathrm{ref}}$, axes of rotor current. The algorithm of the fitness function is represented in Fig. 4.

Firstly, the fitness algorithm receives as parameter the weighting matrices elements, or particle position, $\boldsymbol{W}$ (please see Eq. 23). Secondly, the algorithm executes the simulation using the $\boldsymbol{W}$ values. After the simulation finishes, the vectors for currents references and rotor currents are used as simulation outputs. Analyzing these data, the characteristics of the step response, including ITAE, overshoot, and settling time, must be calculated. Finally, with step response parameters, the fitness value is calculated.

B. PARTICLES MOTION

On each iteration, particles moves using a combination of the best personal experience, denoted by subscript 'pbest', the best global experience, denoted by the subscript, 'gbest', and its actual velocity, $\boldsymbol{W}_{\mathrm{vel}}(k)$, as is explained in [46], [51]–[53]. Thus, next velocity component, $W_{\mathrm{vel},i}$, of current particle, j, is defined as follows:

$$
\begin{aligned}
W^{j}_{\text{vel},i}&(k+1)\\
&= \underbrace{w_{\text{PSO}}(k)\cdot W^{j}_{\text{vel},i}(k)}_{\text{Actual velocity component}}\\
&\quad + \underbrace{c_p\cdot \text{rand}\left([1,0]\right)\left(W^{j}_{\text{pbest},i}(k)-W^{j}_{i}(k)\right)}_{\text{Best personal experience component}}\\
&\quad + \underbrace{c_g\cdot \text{rand}\left([1,0]\right)\left(W_{\text{gbest},i}(k)-W^{j}_{i}(k)\right)}_{\text{Best global experience component}} \qquad (25)
\end{aligned}
$$

and next position component is given by:

$$W^{j}_{i}(k+1) = W^{j}_{i}(k) + W^{j}_{\text{vel},i}(k+1) \qquad (26)$$

In Equation (25), rand ([1, 0]) represents a random uniform number between 0 and 1, $c_g = 1.5$ and $c_p = 1.5$ are the social and cognitive acceleration factors, and $w_{\text{PSO}}(k)$ is the actual adaptive inertia proposed by [38].

The time-varying inertia $w_{\text{PSO}}(k)$ is focused on the exploration when each particle's best personal position is near to another particle, otherwise, its inertia decreases, reversing the trend to the minimization. Thus, the actual inertia is given by:

$$w_{\text{PSO}}(k) = 0.9 - 0.4\frac{d(k)}{\max\left(\{d(k)\}_{1\le k\le k_{\max}}\right)} \qquad (27)$$

Here $k_{\max}$ is the maximum number of iterations and $d(k)$ is the maximum standard deviation between $\boldsymbol{W}^{j}_{i}$, where j represents each particle of the population.

$$d(k) = \max\left(\left\{\text{std}\left(\left\{W^{j}_{\text{pbest},i}\right\}_{1\le j\le \text{P}_{\text{size}}}\right)\right\}_{1\le i\le 8}\right) \qquad (28)$$

where P_{size} is the population size and i refers to each $\boldsymbol{W}^{j}_{\text{pbest}}$ component.

Finally, to clamp down all particle within $\mathbb{S}$ search space a simple method presented in [37] is used. $\mathbb{S}$ is limited to the lower bond $[\,150,-300,-300,150,10^{-9},-10^{-1},-10^{-1},10^{-9}\,]^T$ and to the upper bound $[\,10^{4},300,300,10^{4},1,10^{-1},10^{-1},1\,]^T$. Basically, if a certain particle, with position $\boldsymbol{W}^{j}$, goes outside of the function domain, its violated position component W^{j}_{i} is recalculated once again using Equation (29).

$$W^{j}_{i} = \frac{W^{j}_{\text{pbest},i} + W_{\text{gbest},i} + W^{r1}_{\text{pbest},i} + W^{r2}_{\text{pbest},i}}{4} \qquad (29)$$

superscripts $r1$ and $r2$ represent two randomly selected particles within swarm population.

C. DYNAMIC-OBJECTIVE CONSTRAINT-HANDLING METHOD

The essence of DOCHM is to divide the constrained optimization problem into two unconstrained objectives. The primary objective function, $\Phi(\boldsymbol{W})$, is related constraints:

$$
\begin{aligned}
\phi(\boldsymbol{W}) &= \max\left(\left\{0, \boldsymbol{M}_{p,d}-35\right\}\right) + \max\left(\left\{0, \boldsymbol{M}_{p,q}-35\right\}\right)\\
&\quad + \max\left(\left\{0, \boldsymbol{t}_{ss,d}-3\right\}\right) + \max\left(\left\{0, \boldsymbol{t}_{ss,q}-3\right\}\right) \qquad (30)
\end{aligned}
$$

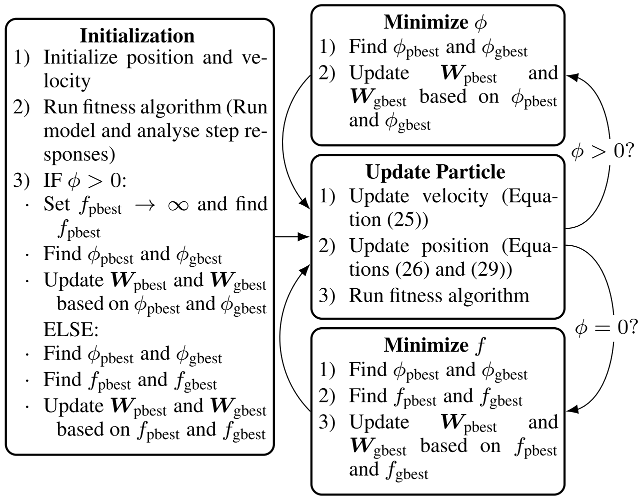

FIGURE 5. PSO with DOCHM pseudo-code state-machine diagram.

$\phi(\boldsymbol{W})$ represents how far the particle is from the feasible region. Thus, if $\phi(\boldsymbol{W}) > 0$ at least one constraint is active and $\phi(\boldsymbol{W})$ must be minimized. In contrast, if $\phi(\boldsymbol{W}) = 0$, then the particle is inside of the feasible region and the minimization process changes to secondary objective function, $f(\boldsymbol{W})$, that is related to the optimization problem without constraints.

$$f(\boldsymbol{W}) = \max\left(\left\{\text{ITAE}_d, \text{ITAE}_q\right\}\right) \qquad (31)$$

Eventually, during the optimization process, a particle can go outside of the feasible region and the minimization process returns to the primary objective function, but, as $\phi(\boldsymbol{W})$ comes back to zero again, the minimization returns to $f(\boldsymbol{W})$, and this loop repeats every time.

The PSO based DOCHM algorithm is present in Fig. 5.

IV. RESULTS OF WDOCHM-PSO ALGORITHM

The WDOCHM-PSO, the fitness algorithms, and the model used for its calculations were built using MATLAB/Simulink. For this model, a constant switching frequency equal to 10^{-4} seconds was used. The mechanical speed ω_m was equal to 1690 rpm, the control and prediction horizons were equal to $N_y = 20$ and $N_u = 10$. The computational time is near to 16 μs, or 6.25 times the switching frequency [54], besides the DFIG parameters are also presented in Table 1.

According to [46], the suggested number of population is 2 to 5 times the dimension of the problem, and some works use 300 as the maximum number of iterations [55], [56]. Therefore, since each particle is a high-fidelity model, which means a high-cost particle, the PSO population $\text{P}_{\text{size}} = 16$ particles, and the maximum number of iterations was $k_{\max} = 300$, which takes approximately two days in an Intel Core i7 and 8 GB of RAM computer.

Fig. 6 describes the progress of $\phi(\boldsymbol{W})$ and $f(\boldsymbol{W})$. Initially, all particles are outside of the feasible region, so $f_{\text{gbest}} \to \infty$. After the 21[st] iteration, one particle reached to $\phi(\boldsymbol{W}) = 0$, (or $\log(\phi(\boldsymbol{W}) = 0) \to -\infty$) and f_{gbest} decreases from infinity to a 1565.7. Therefore, after the optimal value of

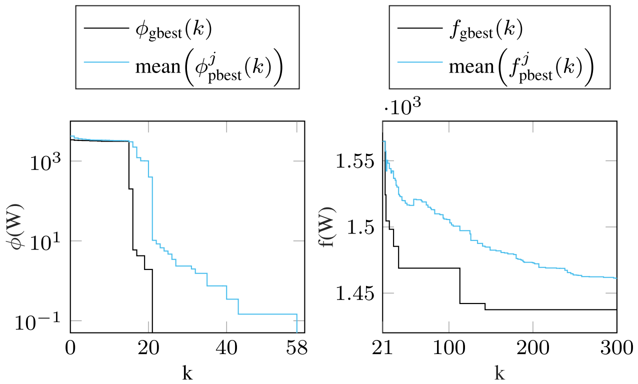

(a) Primary objective function. (b) Secondary objective function.

FIGURE 6. The progress of $\phi(W)$ and $f(W)$ as the number of iteration increases.

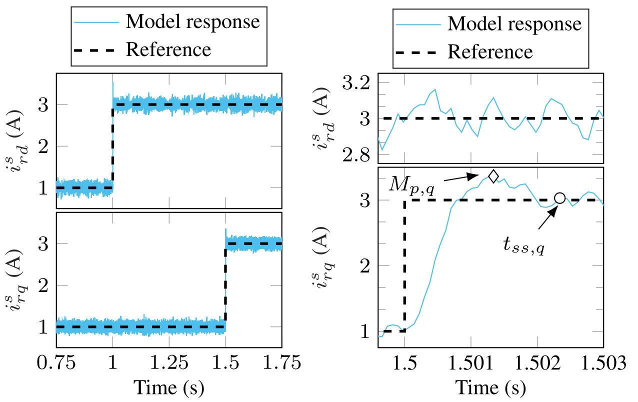

(a) Full overview. (b) Detail under i^s_{rq} step response.

FIGURE 7. Simulated result for WDOCHM-PSO solution of W.

$\phi(W) = 0$ was found, there is a tendency to more particles go to this region and the mean of all ϕ^j_{pbest} decreases. After the 57th iteration all $\phi^j_{\text{pbest}} = 0$.

Also, the solution found by WDOCHM-PSO Method, was presented by:

$$W_{\text{opt}} = \begin{bmatrix} 365 \\ -299 \\ 212 \\ 742 \\ 9 \times 10^{-3} \\ -3 \times 10^{-2} \\ -2 \times 10^{-2} \\ 9.5 \times 10^{-3} \end{bmatrix} \tag{32}$$

and the corresponding response is given in Fig. 7, where Fig.7a indicates the full overview of both direct and quadrature responses, and Fig.7b shows the detail under i^s_{rq} step response. In Fig. 7b, the estimated settling time for quadrature current was $t_{ss,q} = 2.34$ ms and the overshoot for quadrature, $M_{p,q} = 20.47\%$.

Finally, Fig. 8 presents the model working in other situations of active and reactive power generation, as $P_s = 0$

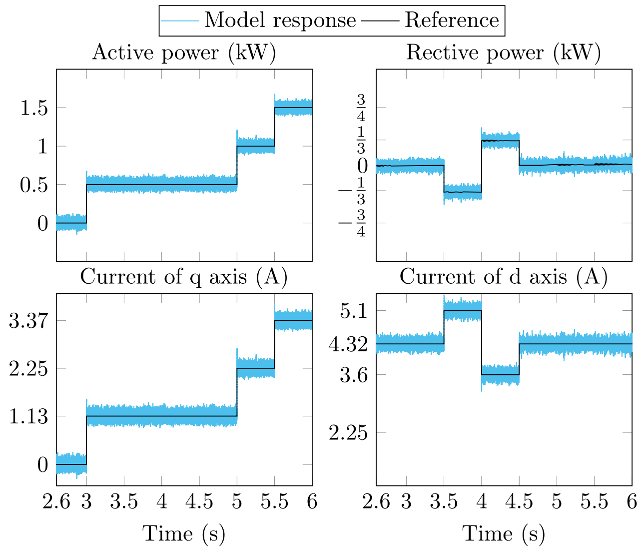

FIGURE 8. Model working for some power generation and the corresponding current.

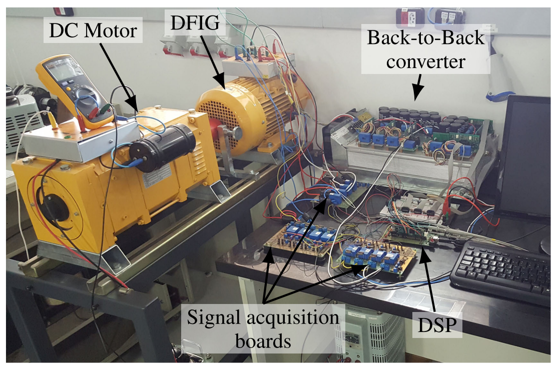

FIGURE 9. Workbench used to get experimental results.

and $Q_s = 0$. Also, Fig. 8 shows the corresponding current of direct and quadrature components for the generated power.

V. EXPERIMENTAL RESULTS

An experimental workbench was used to validate the design of weighting matrices and the theory presented in previous sections (Fig. 9). This workbench includes a Digital Signal Processor (DSP) TMS320F28335, a data acquisition board, a DC motor used to emulate the wind speed, a back-to-back converter and a 3 kW DFIG. The sampling time is the same value of the space vector modulation frequency (10 kHz). The speed is measured by using a 3600 PPR encoder. Moreover, DFIG parameters are presented in Table 1.

A. CONSTANT MECHANICAL SPEED OPERATION

Firstly, the same steps signals used as PSO Model references (Fig. 7) were used here, in order to test the performance of the proposal. In this way, the $i_{rd,\text{ref}}$ and $i_{rq,\text{ref}}$ changed from 1 A to 3 A and the speed is 1690 rpm as depicted in Figure 10. It can be noted that the proposed MBPC, using the

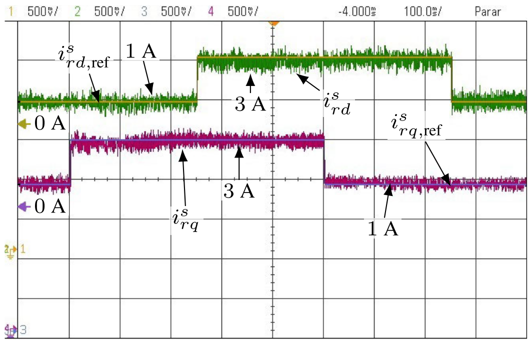

(a) Full overview.

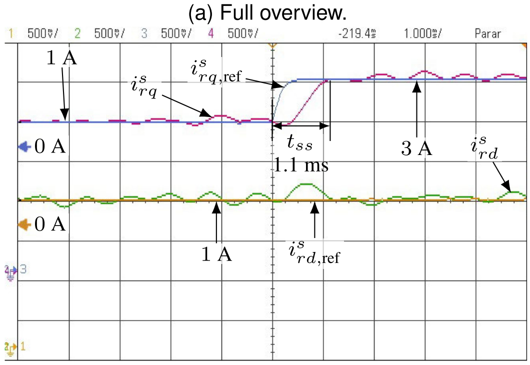

(b) Detail under i^s_{rq} step response.

FIGURE 10. **Step responses of the proposal.**

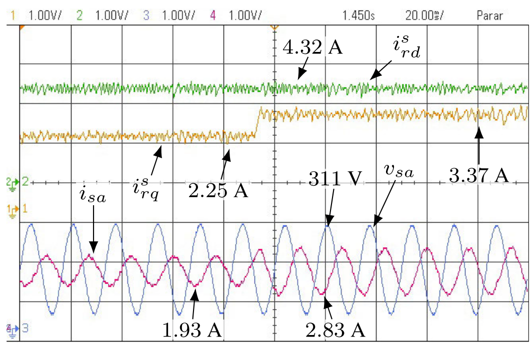

(a) Varying active power while reactive power is constant.

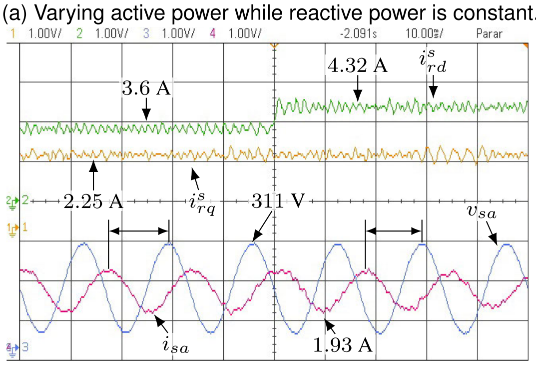

(b) Varying reactive power while active power is constant.

FIGURE 11. **Stator voltage, v_{sa}, and current, i_{sa}, and rotor synchronous components, i^s_{rd} and i^s_{rq} behavior during a step test.**

incremental space-state model and the PSO application to the weighting matrices, allows controlling the rotor current components. The quadrature settling time, $t_{ss,q} = 1.1$ ms,

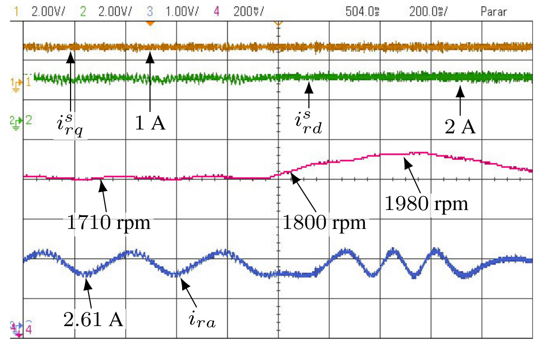

FIGURE 12. **Test for several mechanical speed operation.**

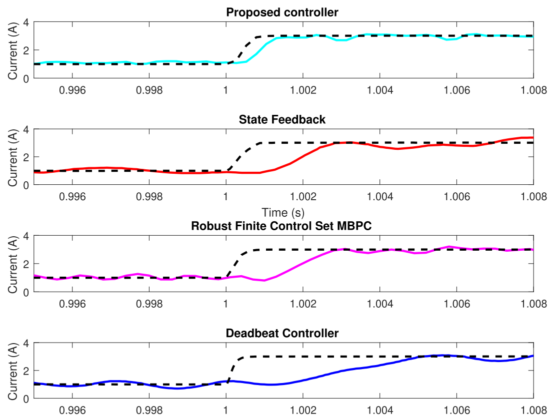

FIGURE 13. **Comparison with the proposed controller and other approaches.**

is better than the result shown in the simulated case as is depicted in Figure 10.

B. COMPARING ROTOR CURRENT COMPONENTS AND GENERATED POWER

In the second test, the behavior of the Phase A stator voltage v_{sa} and current, i_{sa}, is presented during a change in the rotor current references i^s_{rd} and i^s_{rq}. Fig. 11 presents the case where i^s_{rq} changes from 2.25 A to 3.37 A, while i^s_{rd} A keeps constant at 4.32 A. When the stator current amplitude rises from 1.93 A to 2.83 A, then, a consequent increment in the active power from -864 W to -1295 W can be noticed.

Moreover, the reactive power keeps constant at $Q_s = 266$ var. In the same way, Fig. 11b represents another scenario where i^s_{rd} was varied from 3.6 A to 4.32 A, while i^s_{rq} remains constant at 2.25 A. Therefore, a decrease in the reactive power from 543 var to 266 var is produced, while the active power was kept constant at $P_s = -864$ W. Again, in both cases, the proposed MBPC, using the PSO to design the weighting matrices, controls the rotor current in a right way.

C. SEVERAL MECHANICAL SPEED OPERATION

In the third experiment, both rotor currents keep constant at $i^s_{rd} = 2$ A and $i^s_{rq} = 1$ A, while the rotor speed ω_m, varying from 1710 rpm to 1980 rpm (please see Fig. 12), since

TABLE 1. DFIG parameters.

Parameter	Value
Stator resistance per phase (R_s)	1 Ω
Stator inductance per phase (L_s)	0.2010 H
Rotor resistance per phase (R_r)	3.122 Ω
Rotor inductance per phase (L_r)	0.2010 H
Mutual inductance (L_m)	0.1917 H
Synchronous stator speed (ω_s)	120π rad/s
Pole pairs (p)	2
Nominal Active Power (P_s)	3 kW
Nominal Stator Voltage (V_s)	$220/380$ $\Delta - Y$ V
Nominal Stator Flux (λ_s)	0.8249 Wb
DC-link volage (V_{cc})	127 V
Nominal Rotor Voltage (V_r)	440 Y V

the rotor speed is related with the rotor current frequency i_{ra}. In fact, when $\omega_m = 1800$ rpm, or $\omega_{sl} = 0$ the rotor current waveform is a DC signal. Also, it can be seen that this proposal well-works when the rotor speed changes owing to the fact the MBPC controller reaches its references.

D. COMPARISON WITH OTHER CONTROLLERS

In this section, a comparison between the proposed controller with other alternatives presents in the literature is done. Figure 13 shows that comparison using the same step response presented in Figure 10 and the State Feedback controller depicted in [57], the Robust Finite Control Set proposed in [58] and the deadbeat controller described in [59]. It can be noticed that the proposed controller is nearly two times faster and exhibits less settling time than the other ones.

VI. CONCLUSION

In this paper, a methodology for designing the weighting matrices of an MBPC's cost function using WDOCHM-PSO was proposed. As many artificial intelligence methods, the WDOCHM-PSO is very flexible and it can be adapted to project many other controllers easily, whether linear or nonlinear, model-based or not, since the proposed fitness uses non-linear simulations as the main component. Good quality parameters, considering the designer requirements, were achieved, because the settling time and the overshoot of the step response were lower than the maximum specification. For this WDOCHM-PSO, none noise restrictions were directly considered, because, in its inner response, the solution is obtained with the ITAE minor value. And according to [60], the solution of this controller should indirectly minimize the noise.

The advantage of using an off-line algorithm to optimize the MBPC cost function is that there is no limited time to process the algorithm, thus, more complex models can be used during the optimization process. On the other hand, due to the DSP time limitations, it was proposed a simple incremental predictive model without the flux component. As a result, the analyzed response for the experimental case was under the defined constraints and faster than the optimal of the simulated model. Therefore, the off-line optimization method using PSO attended the expectations and it can be used to design MPBC weighting matrices.

Finally, it is possible to use this WDOCHM-PSO tunning approach in other situations. For doing that, it is necessary to change the fitness function, including the model and/or simulation, the fitness calculation processing, and constraints.

APPENDIX

See Table 1.

REFERENCES

[1] A. A. B. M. Zin, M. H. A. Pesaran, A. B. Khairuddin, L. Jahanshaloo, and O. Shariati, "An overview on doubly fed induction generators' controls and contributions to wind based electricity generation," *Renew. Sustain. Energy Rev.*, vol. 27, pp. 692–708, Nov. 2013.

[2] F. Blaabjerg and K. Ma, "Wind energy systems," *Proc. IEEE*, vol. 106, no. 11, pp. 2116–2131, Nov. 2017.

[3] X. Wang and D. Sun, "Three-vector-based low-complexity model predictive direct power control strategy for doubly fed induction generators," *IEEE Trans. Power Electron.*, vol. 32, no. 1, pp. 773–782, Jan. 2017.

[4] G. Abad, J. Lopez, M. Rodríguez, L. Marroyo, and G. Iwanski, *Doubly Fed Induction Machine: Modeling and Control for Wind Energy Generation*. Hoboken, NJ, USA: Wiley, 2011.

[5] E. Tremblay, S. Atayde, and A. Chandra, "Comparative study of control strategies for the doubly fed induction generator in wind energy conversion systems: A DSP-based implementation approach," *IEEE Trans. Sustain. Energy*, vol. 2, no. 3, pp. 288–299, Jul. 2011.

[6] R. Franco, C. E. Capovilla, R. V. Jacomini, J. A. T. Altana, and A. J. S. Filho, "A deadbeat direct power control applied to doubly-fed induction aerogenerator under normal and sag voltages conditions," in *Proc. 40th Annu. Conf. IEEE Ind. Electron. Soc. (IECON)*, Oct. 2014, pp. 1906–1911.

[7] J. S. Solís-Chaves, M. S. Barreto, M. B. C. Salles, V. M. Lira, R. V. Jacomini, and A. J. S. Filho, "A direct power control for DFIG under a three phase symmetrical voltage sag condition," *Control Eng. Pract.*, vol. 65, pp. 48–58, Aug. 2017.

[8] W. Zhi-Nong, Y. Xiao-Yong, W. Jia-Jia, H. Lian-Shan, X. Xiang, C. Dan, and W. Yue, "The intelligent control of DFIG-based wind generation," in *Proc. Int. Conf. Sustain. Power Gener. Supply*, 2009, pp. 1–5.

[9] C. M. Rocha-Osorio, J. S. Solís-Chaves, L. L. Rodrigues, J. L. A. Puma, and A. J. S. Filho, "Deadbeat–fuzzy controller for the power control of a doubly fed induction generator based wind power system," *ISA Trans.*, vol. 88, pp. 258–267, May 2019.

[10] B. Hamane, M. L. Doumbia, A. M. Bouhamida, and M. Benghanem, "Direct active and reactive power control of DFIG based WECS using PI and sliding mode controllers," in *Proc. 40th Annu. Conf. IEEE Ind. Electron. Soc. (IECON)*, Oct. 2014, pp. 2050–2055.

[11] J. S. Solís-Chaves, L. L. Rodrigues, C. M. Rocha-Osorio, and A. J. S. Filho, "A long-range generalized predictive control algorithm for a DFIG based wind energy system," *IEEE/CAA J. Autom. Sinica*, vol. 6, no. 5, pp. 1209–1219, Sep. 2019.

[12] V. Nevistić and J. A. Primbs, "Finite receding horizon linear quadratic control: A unifying theory for stability and performance analysis," California Inst. Technol., Pasadena, CA, USA, Tech. Rep. CaltechCDSTR:1997.001, 1997.

[13] A. Boulahia, M. Adel, and H. Benalla, "Predictive power control of grid and rotor side converters in doubly fed induction generators based wind turbine," *Bull. Electr. Eng. Informat.*, vol. 2, no. 4, pp. 287–293, Dec. 2013.

[14] P. Kou, D. Liang, J. Li, L. Gao, and Q. Ze, "Finite-control-set model predictive control for DFIG wind turbines," *IEEE Trans. Autom. Sci. Eng.*, vol. 15, no. 3, pp. 1004–1013, Jul. 2018.

[15] S. Vazquez, J. Rodriguez, M. Rivera, L. G. Franquelo, and M. Norambuena, "Model predictive control for power converters and drives: Advances and trends," *IEEE Trans. Ind. Electron.*, vol. 64, no. 2, pp. 935–947, Feb. 2017.

[16] A. J. S. Filho, M. E. de Oliveira Filho, and E. R. Filho, "A predictive power control for wind energy," *IEEE Trans. Sustain. Energy*, vol. 2, no. 1, pp. 97–105, Jan. 2011.

[17] X.-B. Kong, L. Wang, and X.-J. Liu, "Predictive control for DFIG-based wind power generation," in *Proc. 24th Chin. Control Decis. Conf. (CCDC)*, May 2012, pp. 240–245.

[18] S. V. Dias, W. A. Silva, T. R. F. Neto, L. L. N. dos Reis, B. C. Torrico, and J. C. T. Campos, "Robust generalized predictive control applied to the mitigation of electromagnetic torque oscillations in a wind energy conversion system based on DFIG," in *Proc. IEEE Biennial Congr. Argentina (ARGENCON)*, Jun. 2016, pp. 1–6.

[19] S. V. Dias, T. R. F. Neto, L. L. N. dos Reis, B. C. Torrico, and J. C. T. Campos, "Robust analysis of a predictive controller of DFIG wind energy systems," in *Proc. IEEE 8th Int. Symp. Power Electron. Distrib. Gener. Syst. (PEDG)*, Apr. 2017, pp. 1–5.

[20] K. Ouari, T. Rekioua, and M. Ouhrouche, "Nonlinear model predictive controller of a variable speed wind turbine driven doubly fed induction generator," *J. Elect. Syst.*, vol. 9, no. 2, pp. 243–255, 2013.

[21] R. Errouissi, A. Al-Durra, S. M. Muyeen, S. Leng, and F. Blaabjerg, "Offset-free direct power control of DFIG under continuous-time model predictive control," *IEEE Trans. Power Electron.*, vol. 32, no. 3, pp. 2265–2277, Mar. 2017.

[22] A. Ahmad and P. Lima, "Multi-robot cooperative spherical-object tracking in 3D space based on particle filters," *Robot. Auton. Syst.*, vol. 61, no. 10, pp. 1084–1093, Oct. 2013.

[23] T. P. Nascimento, C. E. T. Dórea, and L. M. G. Gonçalves, "Nonholonomic mobile robots' trajectory tracking model predictive control: A survey," *Robotica*, vol. 36, no. 5, pp. 676–696, Jan. 2018.

[24] W. Gu, J. Yao, Z. Yao, and J. Zheng, "Output feedback model predictive control of hydraulic systems with disturbances compensation," *ISA Trans.*, vol. 88, pp. 216–224, May 2019.

[25] S. Saeidi, R. A. de Marchi, and E. Bim, "Nonlinear predictive control for a DFIG under voltage dip," in *Proc. 42nd Annu. Conf. IEEE Ind. Electron. Soc. (IECON)*, Oct. 2016, pp. 1955–1960.

[26] A. El Kachani, E. M. Chakir, A. A. Laachir, T. Jarou, and A. Hadjoudja, "Nonlinear model predictive control applied to a DFIG-based wind turbine with a shunt APF," in *Proc. Int. Renew. Sustain. Energy Conf. (IRSEC)*, Nov. 2016, pp. 369–375.

[27] J. Yao, Z. Jiao, and D. Ma, "Adaptive robust control of DC motors with extended state observer," *IEEE Trans. Ind. Electron.*, vol. 61, no. 7, pp. 3630–3637, Jul. 2014.

[28] R. Kennel, A. Linder, and M. Linke, "Generalized predictive control (GPC)-ready for use in drive applications?" in *Proc. IEEE 32nd Annu. Power Electron. Spec. Conf.*, vol. 4, Jun. 2001, pp. 1839–1844.

[29] M. W. Naouar, A. A. Naassani, E. Monmasson, and I. S. Belkhodja, "FPGA-based predictive current controllerfor synchronous machine speed drive," *IEEE Trans. Power Electron.*, vol. 23, no. 4, pp. 2115–2126, Jul. 2008.

[30] L. G. Bleris, P. D. Vouzis, M. G. Arnold, and M. V. Kothare, "A co-processor FPGA platform for the implementation of real-time model predictive control," in *Proc. Amer. Control Conf.*, 2006, pp. 1–6.

[31] J. A. Rossiter, *Model-Based Predictive Control: A Practical Approach*. Boca Raton, FL, USA: CRC Press, 2003.

[32] H. Liu, W. Sung, and W. Yao, *Computer, Intelligent Computing and Education Technology*. Boca Raton, FL, USA: CRC Press, 2014.

[33] Y. Bekakra and D. B. Attous, "Optimal tuning of PI controller using PSO optimization for indirect power control for DFIG based wind turbine with MPPT," *Int. J. Syst. Assurance Eng. Manage.*, vol. 5, no. 3, pp. 219–229, Sep. 2014.

[34] O. P. Bharti, R. K. Saket, and S. K. Nagar, "Controller design for doubly fed induction generator using particle swarm optimization technique," *Renew. Energy*, vol. 114, pp. 1394–1406, Dec. 2017.

[35] R. Ruiz-Cruz, E. N. Sanchez, F. Ornelas-Tellez, A. G. Loukianov, and R. G. Harley, "Particle swarm optimization for discrete-time inverse optimal control of a doubly fed induction generator," *IEEE Trans. Cybern.*, vol. 43, no. 6, pp. 1698–1709, Dec. 2013.

[36] J.-H. Chen, H.-T. Yau, and W. Hung, "Design and study on sliding mode extremum seeking control of the chaos embedded particle swarm optimization for maximum power point tracking in wind power systems," *Energies*, vol. 7, no. 3, pp. 1706–1720, Mar. 2014.

[37] H. Lu and W. Chen, "Dynamic-objective particle swarm optimization for constrained optimization problems," *J. Combinat. Optim.*, vol. 12, no. 4, pp. 409–419, Oct. 2006.

[38] S. Kessentini and D. Barchiesi, "Particle swarm optimization with adaptive inertia weight," *Int. J. Mach. Learn. Comput.*, vol. 5, no. 5, pp. 368–373, Oct. 2015.

[39] L. Fan and Z. Miao, *Modeling and Analysis of Doubly Fed Induction Generator Wind Energy Systems*. New York, NY, USA: Academic, 2015.

[40] A. L. L. F. Murari, J. A. T. Altuna, K. A. C. Chirapo, A. Pelizari, and A. J. S. Filho, "Electromagnetic core analysis of a DFIG state-feedback power controller," *J. Microw., Optoelectron. Electromagn. Appl.*, vol. 18, no. 3, pp. 343–357, Jul. 2019.

[41] D. M. Prett and C. E. García, *Fundamental Process Control*. Amsterdam, The Netherlands: Elsevier, 2013.

[42] M. Ramzi, H. Youlal, and M. Haloua, "State space model predictive control of an aerothermic process with actuators constraints," *Intell. Control Autom.*, vol. 3, no. 1, pp. 50–58, 2012.

[43] E. F. Camacho and C. Bordons, *Model Predictive Control*, 2nd ed. London, U.K.: Springer-Verlag, 2004.

[44] J. M. Maciejowski, *Predictive Control: With Constraints*. London, U.K.: Pearson, 2002.

[45] K. Ogata, *Discrete-Time Control Systems*, vol. 2. Englewood Cliffs, NJ, USA: Prentice-Hall, 1995.

[46] M. Pant, R. Thangaraj, and A. Abraham, *Foundations of Computational Intelligence: Global Optimization*, vol. 3. Cham, Switzerland: Springer-Verlag, 2009.

[47] H. Shayeghi, A. Safari, and H. A. Shayanfar, "PSS and TCSC damping controller coordinated design using PSO in multi-machine power system," *Energy Convers. Manage.*, vol. 51, no. 12, pp. 2930–2937, Dec. 2010.

[48] E. S. Ali and S. M. Abd-Elazim, "Bacteria foraging optimization algorithm based load frequency controller for interconnected power system," *Int. J. Elect. Power Energy Syst.*, vol. 33, no. 3, pp. 633–638, Mar. 2011.

[49] D. Maiti, A. Acharya, M. Chakraborty, A. Konar, and R. Janarthanan, "Tuning pid and pi$^{\lambda}$d$^{\delta}$ controllers using the integral time absolute error criterion," in *Proc. 4th Int. Conf. Inf. Automat. Sustainability*, Dec. 2008, pp. 457–462.

[50] S. Panda and N. P. Padhy, "Thyristor controlled series compensator-based controller design employing genetic algorithm: A comparative study," *Int. J. Electron., Circuits Syst.*, vol. 1, no. 1, pp. 38–47, 2007.

[51] H. Lu and W. Chen, "Self-adaptive velocity particle swarm optimization for solving constrained optimization problems," *J. Global Optim.*, vol. 41, no. 3, pp. 427–445, Jul. 2008.

[52] S. Ebbesen, P. Kiwitz, and L. Guzzella, "A generic particle swarm optimization MATLAB function," in *Proc. Amer. Control Conf. (ACC)*, Jun. 2012, pp. 1519–1524.

[53] V. R. Kulkarni and V. Desai, "ABC and PSO: A comparative analysis," in *Proc. IEEE Int. Conf. Comput. Intell. Comput. Res. (ICCIC)*, Dec. 2016, pp. 1–7.

[54] L. L. Rodrigues, O. A. C. Vilcanqui, A. L. L. F. Murari, and A. J. S. Filho, "Predictive power control for DFIG: A FARE-based weighting matrices approach," *IEEE J. Emerg. Sel. Topics Power Electron.*, vol. 7, no. 2, pp. 967–975, Jun. 2019.

[55] A. Y. Galan, R. Sauleau, and A. V. Boriskin, "Parameter selection in particle swarm optimization algorithm for synthesis of linear arrays with flat-top beams," *Telecommun. Radio Eng.*, vol. 70, no. 16, pp. 1415–1428, 2011.

[56] A. A. El-Saleh, M. Ismail, M. Akbari, M. R. Manesh, and S. A. R. T. Zavareh, "Minimizing the detection error of cognitive radio networks using particle swarm optimization," in *Proc. Int. Conf. Comput. Commun. Eng. (ICCCE)*, Jul. 2012, pp. 877–881.

[57] J. S. Filho, A. L. de Lacerda Ferreira Murari, C. E. Capovilla, J. A. T. Altuna, and R. V. Jacomini, "A state feedback DFIG power control for wind generation," *Eletrônica Potência*, vol. 20, no. 2, pp. 151–159, May 2015.

[58] A. J. S. Filho, A. L. de Oliveira, L. L. Rodrigues, E. C. M. Costa, and R. V. Jacomini, "A robust finite control set applied to the DFIG power control," *IEEE J. Emerg. Sel. Topics Power Electron.*, vol. 6, no. 4, pp. 1692–1698, Dec. 2018.

[59] L. A. L. de Almeida, A. J. S. Filho, C. E. Capovilla, I. R. S. Casella, and F. F. Costa, "An impulsive noise filter applied in wireless control of wind turbines," *Renew. Energy*, vol. 86, pp. 347–353, Feb. 2016.

[60] C. M. Hackl, *Non-Identifier Based Adaptive Control in Mechatronics: Theory and Application* (Lecture Notes in Control and Information Sciences), vol. 466, 1st ed. Chennai, India: Springer, 2017.

LUCAS LIMA RODRIGUES received the bachelor's degree in electrical engineering from the Federal University of Bahia, Salvador, Brazil, in 2017, and the master's degree in renewable energy and predictive control from the Federal University of ABC (UFABC), Santo André, Brazil. He is currently pursuing the Ph.D. degree in renewable energy and predictive control with the University of São Paulo (USP). He is also a Professor with the Federal University of Acre, Rio Branco, Brazil. His research interests are power electronics, predictive control, renewable energy, doubly-fed induction generators, and meta-heuristic optimization.

J. SEBASTIÁN SOLÍS-CHAVES was born in Ipiales, Nariño, Colombia, in 1980. He received the B.S. degree in electrical engineering and the M.S. degree in industry automation from the Universidad Nacional de Colombia, in 2006 and 2009, respectively, and the Ph.D. degree in energy engineering from the Universidade Federal do ABC (UFABC), in 2017. He has been a full-time Professor with the Universidad Escuela Colombiana de Carreras Industriales (UECCI), Bogotá, Colombia, since 2018. He's teaching in the areas of electrical machines, renewable energies, industry automation, and power electronics. His research interests include control of doubly-fed induction generator for wind energy systems, smart grids, and GIS software for renewable energy applications using the sustainable development perspective.

OMAR A. C. VILCANQUI received the B.S. degree in electrical engineering from the University Nacional of Altiplano, Puno, Perú, in 2006, and the master's and Ph.D. degrees from the Federal University of Bahia, Salvador, Brazil, in 2009 and 2014, respectively. He is currently a Professor of power electronics with the Federal University of Acre, Rio Branco, Brazil. His current research interests include control, signal processing, and power electronics.

ALFEU J. SGUAREZI FILHO (Senior Member, IEEE) received the Ph.D. degree from Campinas University, Brazil, in 2010. He is currently a full-time Professor with the Federal University of ABC (UFABC), Santo André, Brazil, teaching in the areas of electrical machines and power electronics and electrical drives. His research interests are machine drives, wind and photo-voltaic energies, doubly-fed induction generators, power control, and electrical power systems.